DOI: 10.5281/zenodo.23532356

CURRENT DEVELOPMENTS AND THEMATIC REVIEWS IN MATHEMATICS

Editor
Prof. Mustafa Dede, PhD.

Current Developments and Thematic Reviews in Mathematics

Editor

Prof. Mustafa Dede, PhD.

Publisher
Platanus Publishing®

Editor in Chief

Prof. Mustafa Dede, PhD.

Cover & Interior Design
Platanus Publishing®

The First Edition
October, 2026

ISBN

978-625-91284-2-9

©copyright
All rights reserved. No part of this publication may be reproduced or transmitted in any form or by any means, electronic or mechanical, including photocopy, or any information storage or retrieval system, without permission from the publisher.

Platanus Publishing®
Address: Natoyolu Cad. Fahri Korutürk Mah. 157/B, 06480, Mamak, Ankara, Turkey.

Phone: +90 312 390 1 118
web: www.platanuspublishing.com
e-mail: platanuskitap@gmail.com



Platanus Publishing®

CONTENTS

CHAPTER 1 5

New Structure of Diamond Alpha Fractional Inequalities
Yusuf Zeren

CHAPTER 2 19

Nonlinear Diffusion Equations: Mathematical Foundations and Numerical Experiments
Özlem Kaytmaz

CHAPTER 3 37

Küme Değerli Analizde Temel Tanımlar
Gonca İnceoğlu

CHAPTER 1

New Structure of Diamond Alpha Fractional Inequalities

Yusuf Zeren[1]

[1] Prof. Dr., Yıldız Technical University, ORCID: 0000-0001-8346-2208

1. Literature and Basic Structures of Time Scales

Hardy [1] gave the following classical Hardy inequality in 1920. Let (a_n) be a sequence, and let $b > 1$, where $b \in R$.

$$\sum_{i=1}^{\infty}\left(\frac{a_1 + a_2 + a_3 + \cdots + a_i}{i}\right)^c < \left(\frac{b}{b-1}\right)^b \sum_{i=1}^{\infty} a_i^b.$$

In [2], Hardy also gave the following inequality.

$$\int_0^{\infty}\left(\frac{1}{s}\int_0^{s} w(\tau)d\tau\right)^c ds \le \left(\frac{c}{c-1}\right)^c \int_0^{\infty} w^c(s)ds, \qquad (1)$$

where v^b is integrable for $v(\theta) \ge 0$, and $b > 1$.

Later, in [3], Hardy developed the above inequality as follows for $b > 1$, $v(\theta) > 0$, and integrable v on $(0, \infty)$; then the following inequalities hold.

$$\int_0^{\infty}\left(\frac{1}{x^j}\int_x^{\infty} v(\theta)d\theta\right)^b dx \le \left(\frac{b}{1-j}\right)^b \int_0^{\infty} \frac{1}{x^{j-b}} v^b(\theta)d\theta\,, \quad j < 1, \qquad (2)$$

$$\int_0^{\infty}\left(\frac{1}{x^j}\int_0^{x} w(\theta)d\theta\right)^b dx \le \left(\frac{b}{j-1}\right)^b \int_0^{\infty} \frac{1}{x^{j-b}} v^b(x)dx\,, \quad j > 1. \qquad (3)$$

In [4], Hardy and Littlewood obtained the following inequalities for (a_j) and $b > 1$

$$\sum_{j=1}^{\infty}\frac{1}{j^l}\left(\sum_{i=j}^{\infty} a_i\right)^c \le N \sum_{j=1}^{\infty}\frac{1}{j^{l-b}} a_j^b\,, \qquad l < 1,$$

$$\sum_{j=1}^{\infty}\frac{1}{j^l}\left(\sum_{i=1}^{j} a_i\right)^c \le N \sum_{j=1}^{\infty}\frac{1}{j^{l-b}} a_j^b\,, \qquad l > 1,$$

where N is a constant.

In [9], Akın and Zeren gave the fractional Hardy operator and its adjoint on $(0, \infty)$ as $H_c w(x) = \frac{1}{x^{1-c}}\int_0^x w(\theta)d\theta$, and $\widetilde{H}_c w(x) = \int_x^{\infty} \frac{1}{x^{1-c}} w(\theta)d\theta$ for $0 \le c < 1$.

In [1,4], Hardy proved the following inequalities for $c = 0$.

$\int_0^{\infty} |Hw(\tau)|^{\theta} d\tau \le (\theta')^{\theta} \int_0^{\infty} |w(\tau)|^{\theta} d\tau$, and $\int_0^{\infty} \left|\widetilde{H}w(\tau)\right|^{\theta} d\tau \le \theta^{\theta} \int_0^{\infty} |w(\tau)|^{\theta} d\tau$,

where $\theta > 1$ and $1/\theta + 1/\theta' = 1$.

Now, let us present the basic definitions and theorems regarding time scales for the proof of our main result.

The foundations of time scale theory were established by Stefan Hilger in [25]. Since its introduction, the theory has attracted considerable interest, and numerous studies have been devoted to dynamic integral inequalities on time scales, yielding a variety of significant results. This line of research has subsequently evolved into an active and important area of investigation, with applications extending beyond pure and applied mathematics to various other scientific disciplines. For a comprehensive treatment of the theory and its applications, the reader is referred to the monographs [43, 53, 54]. For more details about the literature, see [5-54].

A time scale $\mathbb{T}$ is a nonempty closed subset of the real numbers $\mathbb{R}$. The interval $[c,d]_{\mathbb{T}}$ is denoted by $[c,d] \cap \mathbb{T}$.

Definition 1.1 [53] Two functions $\sigma, \rho: \mathbb{T} \to \mathbb{T}$ are defined by $\sigma(x) = inf\{s \in \mathbb{T}: s > x\}$, $\rho(x) = sup\{s \in \mathbb{T}: s > x\}$ for $x \in \mathbb{T}$. $\sigma(x)$ is the forward jump operator, and $\rho(x)$ is the backward jump operator, respectively. If $\sigma(x) > x$, then x is right-scattered, and if $\sigma(x) = x$, then x is called right-dense. If $\rho(x) < x$, then x is left-scattered, and if $\rho(x) = x$, then x is called left-dense.

Definition 1.2 [53] Two functions $\mu, \vartheta: \mathbb{T} \to \mathbb{R}^+$ such that $\mu(x) = \sigma(x) - x$, $\vartheta(x) = x - \rho(x)$. $\mu(x)$ and $\vartheta(x)$ are called graininess functions.

If $\mathbb{T}$ has a left-scattered maximum i, then $\mathbb{T}^k = \mathbb{T} - \{i\}$. Otherwise $\mathbb{T}^k = \mathbb{T}$. In [43, 53, 54], $\mathbb{T}^{\mathrm{k}}$, $\mathbb{T}_k$ are defined as follows

$$\mathbb{T}^k = \begin{cases} \mathbb{T} \setminus (\rho\, sup\, \mathbb{T}, sup\, \mathbb{T}], & if \quad sup\, \mathbb{T} < \infty \\ \mathbb{T}, & if \quad sup\, \mathbb{T} = \infty, \end{cases}$$

and

$$\mathbb{T}_k = \begin{cases} \mathbb{T} \setminus [inf\, \mathbb{T}, \sigma(inf\, \mathbb{T})], & |inf\, \mathbb{T}| < \infty \\ \mathbb{T}, & inf\, \mathbb{T} = -\infty. \end{cases}$$

Suppose that $\pi: \mathbb{T} \to \mathbb{R}$ is a function. Let x be right-dense.

i) π is Δ −differentiable at point x and continuous at point x.

Also, let π be left-continuous at point x, and x be right-scattered; then π is Δ −differentiable at point x,

$$\pi^{\Delta}(x) = \frac{\pi^{\sigma}(x) - (x)}{\mu(x)}$$

ii) π is Δ −differentiable at point x and $\lim_{t \to x} \frac{\pi(x) - \pi(t)}{x - t}$. Then we have the following equality

$$\pi^{\Delta}(x) = \lim_{t \to x} \frac{\pi(x) - \pi(t)}{x - t}.$$

iii) π is Δ −differentiable at point x. Then we have the following equality $\pi^{\sigma}(x) = \pi(x) + \mu(x)\pi^{\Delta}(x)$.

Remark 1. 3 [54] Let $\mathbb{T} = \mathbb{R}$, then $\pi^{\Delta}(x) = \pi'(x)$, and let $\mathbb{T} = \mathbb{Z}$, then $\pi^{\Delta}(x)$ reduces to $\Delta\pi(x)$.

Definition 1.4 [43] If $\Pi: \mathbb{T} \to \mathbb{R}$ is defined a $\Delta -$ antiderivative of $\pi: \mathbb{T} \to \mathbb{R}$, then $\Pi^{\Delta} = \pi(x)$ holds for all $x, t \in \mathbb{T}$, and we define the Δ −integral of π by

$$\int_{t}^{x} \pi(\theta)\Delta\theta = \Pi(x) - \Pi(t),$$

Definition 1.5 [43] Let $\pi: \mathbb{T}_k \to \mathbb{R}$ be ∇ −differentiable at $x \in \mathbb{T}_k$. If $\epsilon > 0$, then there exists a neighborhood W of x with $t \in W$ such that the following inequality holds

$$\left|\pi\big(\rho(x)\big) - \pi(t) - \pi^{\nabla}(x)(\rho(x) - t)\right| \leq \epsilon|\rho(x) - t|,$$

Definition 1.6 [43] Let $\Pi: \mathbb{T} \to \mathbb{R}$ be ∇ −antiderivative of $\pi: \mathbb{T} \to \mathbb{R}$ for $x, t \in \mathbb{T}$; then we define

$$\int_{t}^{x} \pi(\theta)\nabla\theta = \Pi(x) - \Pi(t),$$

If $g(x)$ is $\diamond_{\propto}$−differentiable on $\mathbb{T}$ for all $x \in \mathbb{T}$ and $\propto \in [0,1]$, then we can define $g^{\diamond\propto}(x)$ by

$$g^{\diamond\propto}(x) = \propto g^{\Delta}(x) + (1-\propto)g^{\nabla}(x).$$

Proposition 1.7 [43] $g, \pi: \mathbb{T} \to \mathbb{R}$ are $\diamond_{\propto}$−differentiable two functions for all $x \in \mathbb{T}$ with $\propto \in [0,1]$, then

(i) $(g + \pi): \mathbb{T} \to \mathbb{R}$ *is* $\diamond_{\propto}$−differentiable $\forall x \in \mathbb{T}$ with $\propto \in [0,1]$

$$(g + \pi)^{\diamond\propto}(x) = g^{\diamond\propto}(x) + \pi^{\diamond\propto}(x).$$

(ii) $kg: \mathbb{T} \to \mathbb{R}$ *is* $\diamond_{\propto}$−differentiable $\forall x \in \mathbb{T}$ with $\propto \in [0,1]$

$$(kg)^{\diamond\propto}(x) = kg^{\diamond\propto}(x),$$

where $x, k \in \mathbb{R}$.

(iii) $g, \pi: \mathbb{T} \to \mathbb{R}$ *is* $\diamond_\propto -$differentiable $\forall x \in \mathbb{T}$ with $\propto \in [0,1]$

$$(g\pi)^{\diamond\propto}(x) = g^{\diamond\propto}(x)\pi(x) + \propto g^{\sigma}(x)\pi^{\Delta}(x) + (1-\propto)g^{\rho}(x)\pi^{\nabla}(x).$$

Definition 1.8 [43] Let $g: \mathbb{T} \to \mathbb{R}$ be $\diamond_\propto -$integrable for all $a, x \in \mathbb{T}$ with $\propto \in [0,1]$, then

$$\int_a^x g(\theta) \diamond_\propto \theta = \propto \int_a^x g(\theta)\Delta\theta + (1-\propto)\int_a^x g(\theta)\nabla\theta$$

Definition 1.9 [42, 52] Let $g \in C_{rd}(\mathbb{T}, \mathbb{R})$, $x \in \mathbb{T}_k^k$ and let $g: \mathbb{T} \to \mathbb{R}$ be $\diamond_\propto -$integrable function; then

$$\int_x^{\sigma(x)} g(\theta) \diamond_\propto \theta = \mu(x)g(x).$$

Definition 1.10 In [43, 51] (Chain Rule) Let $\tau: \mathbb{R} \to \mathbb{R}$ be continuously differentiable. Assume that $\pi: \mathbb{T} \to \mathbb{R}$ is continuous and $\diamond_\propto$-differentiable. Then $\tau \circ \pi: \mathbb{T} \to \mathbb{R}$ is $\diamond_\propto$ - differentiable, and there exists b in the real interval $[c, d]$ such that

$$(\tau \circ \pi)^{\diamond\propto}(\epsilon) = \propto (\tau \circ \pi)^{\Delta}(\epsilon) + (1-\propto)(\tau \circ \pi)^{\nabla}(\epsilon) \qquad (4)$$

Definition 1.11 [43, 51] The partial integration formula on the time scale is given by

$$\int_c^d m(\theta)v^{\diamond\propto}(\theta) \diamond_\propto \theta = m(\theta)v(\theta)\mathrm{I}_c^d - \int_c^d m^{\diamond\propto}(\theta)v^{\sigma}(\theta) \diamond_\propto \theta \qquad (5)$$

with $\propto \in [0,1]$.

Definition 1.12 [48] The Hölder inequality on $\diamond_\propto$ calculus is given by

$$\int_c^d |m(\theta)v(\theta)| \diamond_\propto \theta \leq \left(\int_c^d |m(\theta)|^{\tau} \diamond_\propto \theta\right)^{\frac{1}{\tau}} \cdot \left(\int_c^d |v(\theta)|^{\tau'} \diamond_\propto \theta\right)^{\frac{1}{\tau'}} \qquad (6)$$

where $0 \leq \propto \leq 1$, $1/\tau + 1/\tau' = 1$, $\tau > 1$ and $m, v \in C_{rd}([c, d] \cap \mathbb{T}, \mathbb{R})$.

For the remainder of our work, we will suppose that the functions v_i, φ_i, and δ_i are positive functions and $ld-$continuous. We will also need the following arithmetic-geometric inequality. (see [21])

$$\prod_{i=1}^{n} \vartheta_i^{\,y_i} < \sum_{i=1}^{n} \vartheta_i y_i, \qquad (7)$$

where $\sum_{i=1}^{n} y_i = 1$.

Let us define two operators.

$B_i(\epsilon) = \frac{1}{v_i(\epsilon)}\int_x^z v_i(\theta)\gamma_i(\theta)\delta_i(\theta) \diamond_\propto \theta$, and $K_{i,c}\gamma(\epsilon) = \frac{1}{\epsilon^{1-c}}\int_x^z \gamma_i(\theta) \diamond_\propto \theta$ for $\epsilon \in [x, \infty)_{\mathbb{T}}$ and $i = 1,2, \dots, n$.

2. Main Result

Theorem 2.1. Let $y_j < \vartheta_j$ and $1 < y_j < \varphi_j$ such that $\sum_{l=1}^{i} \vartheta_l = 1$. $\tau_j(x)$ is a non-increasing functions for $l = 1,2,\dots,i$, and $h_l(x)$ is a non-decreasing for $l = 1,2,\dots,i$. Let the constants $\Phi_l > 0$ satisfy

$$\left[\frac{\Pi_{l,c}^{\rho}\Lambda(\epsilon)}{\Pi_{l,c}\Lambda(\epsilon)}\right]^{\frac{\vartheta_l}{y_l}} \frac{\varphi_l \Pi_{l,c}\Lambda(\epsilon)\tau_l{}^{\diamond_\alpha}(\epsilon)}{(\vartheta_l - y_l)\Lambda_l(x)\tau_l(\epsilon)} + 1 \geq \left[\frac{\Pi_{l,c}^{\rho}\Lambda(\epsilon)}{\Pi_{l,c}\Lambda(\epsilon)}\right]^{\frac{\vartheta_l}{y_l}} \frac{\varphi_l \Pi_{l,c}\Lambda(\epsilon)h_l{}^{\diamond_\alpha}(\epsilon)}{(\vartheta_l - y_l)\Lambda_l(x)h_l^{\rho}(\epsilon)} + \frac{1}{\Phi_l}. \quad (8)$$

For constants $A_l > 0$, we have the following inequality

$$\int_r^{\infty} \prod_{l=1}^{i} \left(\left[B_l^{\rho}(\epsilon)\right]^{\varphi_l} \frac{[h_l^{\rho}(\epsilon)\Lambda_l(x)]^{y_l}}{\left[\Pi_{l,c}^{\rho}\Lambda(\epsilon)\right]^{\vartheta_l}} \right) \diamond_\alpha \epsilon$$

$$\leq \left[\prod_{l=1}^{i} \frac{1}{A_l^{\varphi_l}}\right] \sum_{l=1}^{i} C_l \int_r^{\infty} h_l^{\rho}(\epsilon)\Lambda_l(x)\delta_l^{\frac{\varphi_l}{y_l}}(\epsilon) \frac{\left(\Pi_{l,c}^{\rho}\Lambda(\epsilon)\right)^{\frac{\vartheta_l}{y_l}\left(\frac{\varphi_l}{y_l}-1\right)}}{\left(\Pi_{l,c}\Lambda(\epsilon)\right)^{\frac{\varphi_l}{y_l}\left(\frac{\vartheta_l}{y_l}-1\right)}} \diamond_\alpha \epsilon, \quad (9)$$

where $C_l = y_l \left(A_l \frac{\Phi_l \varphi_l}{\vartheta_l - y_l}\right)^{\frac{\varphi_l}{y_l}}$.

Proof. Integrating the left-hand side of (9) for

$$\tau(\epsilon) = -\int_{\epsilon}^{\infty} \Lambda_l(t) \left(\Pi_{l,c}^{\rho}\Lambda(t)\right)^{-\frac{\vartheta_l}{y_l}} \diamond_\alpha t.$$

We obtain the following equality

$$\int_r^{\infty} \frac{h_l^{\rho}(\epsilon)\Lambda_l(\epsilon)\left[B_l^{\rho}(\epsilon)\right]^{\frac{\varphi_l}{y_l}}}{\left(\Pi_{l,c}^{\rho}\Lambda(\epsilon)\right)^{\frac{\vartheta_l}{y_l}}} \diamond_\alpha \epsilon = -\int_r^{\infty} \tau(\epsilon) \left(h_l(\epsilon) B_l^{\frac{\varphi_l}{y_l}}(\epsilon) \right)^{\diamond_\alpha} \diamond_\alpha \epsilon. \quad (10)$$

We use (5) with

$$\begin{bmatrix} \xi^{\rho}(\epsilon) = h_l^{\rho}(\epsilon)\left[B_l^{\rho}(\epsilon)\right]^{\frac{\varphi_l}{y_l}} \\ \tau^{\diamond_\alpha}(\epsilon) = \dfrac{\Lambda_l(\epsilon)}{\left(\Pi_{l,c}^{\rho}\Lambda(\epsilon)\right)^{\frac{\vartheta_l}{y_l}}} \end{bmatrix},$$

to obtain

$$\int_r^{\infty} \frac{h_l^{\rho}(\epsilon)\Lambda_l(\epsilon)\left[B_l^{\rho}(\epsilon)\right]^{\frac{\varphi_l}{y_l}}}{\left(\Pi_{l,c}^{\rho}\Lambda(\epsilon)\right)^{\frac{\vartheta_l}{y_l}}} \diamond_\alpha \epsilon$$

$$= \tau(x) h_l(\epsilon) B_l^{\frac{\varphi_l}{y_l}}(\epsilon) I_r^{\infty} - \int_r^{\infty} \tau(\epsilon) \left(h_l(\epsilon) B_l^{\frac{\varphi_l}{y_l}}(\epsilon) \right)^{\diamond_\alpha} \diamond_\alpha \epsilon.$$

From (4), we obtain the following inequality

$$\left(\left(\Pi_{l,c}\Lambda(t)\right)^{1-\frac{\vartheta_l}{y_l}}\right)^{\diamond_\propto} = \left(1-\frac{\vartheta_l}{y_l}\right)\Pi_{l,c}^{\diamond_\propto}\Lambda(t)\int_0^1 \left(\theta\Pi_{l,c}^{\rho}\Lambda(t)+(1-\theta)\Pi_{l,c}(t)\right)^{-\frac{\vartheta_l}{y_l}} \diamond_\propto \theta$$

$$\leq \left(1-\frac{\vartheta_l}{y_l}\right)\Pi_{l,c}^{\diamond_\propto}\Lambda(t)\int_0^1 \left(\theta\Pi_{l,c}^{\rho}\Lambda(t)+(1-\theta)\Pi_{l,c}\Lambda(t)\right)^{-\frac{\vartheta_l}{y_l}} \diamond_\propto \theta$$

$$= \left(1-\frac{\vartheta_l}{y_l}\right)\left(\Pi_{l,c}^{\rho}\Lambda(t)\right)^{-\frac{\vartheta_l}{y_l}}\Lambda_l(t),$$

So, we obtain the following inequality

$$\left(\Pi_{l,c}^{\rho}\Lambda(t)\right)^{-\frac{\vartheta_l}{y_l}}\Lambda_l(t) \leq \frac{y_j}{y_j-\vartheta_j}\left(\left(\Pi_{l,c}\Lambda(t)\right)^{1-\frac{\vartheta_l}{y_l}}\right)^{\diamond_\propto}.$$

Therefore

$$\tau(\epsilon) = -\int_{\epsilon}^{\infty}\left(\Pi_{l,c}^{\rho}\Lambda(t)\right)^{-\frac{\vartheta_l}{y_l}}\Lambda_l(t) \diamond_\propto t \leq \frac{y_l}{y_l-\vartheta_l}\int_{\epsilon}^{\infty}\left(\left(\Pi_{l,c}\Lambda(t)\right)^{1-\frac{\vartheta_l}{y_l}}\right)^{\diamond_\propto} \diamond_\propto t$$

$$= \frac{y_l}{\vartheta_l-y_l}\left(\left(\Pi_{l,c}\Lambda(t)\right)^{1-\frac{\vartheta_l}{y_l}} - I_l\right) \leq \frac{y_l}{\vartheta_l-y_l}\left(\Pi_{l,c}\Lambda(t)\right)^{1-\frac{\vartheta_l}{y_l}}. \qquad (11)$$

Combining (10) and (11),

$$\int_r^{\infty}\frac{h_l^{\rho}(\epsilon)\Lambda_l(\epsilon)\left[B_l^{\rho}(\epsilon)\right]^{\frac{\vartheta_l}{y_l}}}{\left(\Pi_{l,c}^{\rho}\Lambda(\epsilon)\right)^{-\frac{\vartheta_l}{y_l}}} \diamond_\propto \epsilon$$

$$\leq \frac{y_l}{\vartheta_l-y_l}\int_r^{\infty}\left(\Pi_{l,c}\Lambda(\epsilon)\right)^{1-\frac{\vartheta_l}{y_l}}\left(h_l(\epsilon)B_l^{\frac{\varphi_l}{y_l}}(\epsilon)\right)^{\diamond_\propto} \diamond_\propto \epsilon. \qquad (12)$$

From $B_l(\epsilon)$, we obtain the following equation

$$B_l^{\diamond_\propto}(\epsilon) = \frac{[\tau_l(\epsilon)\Lambda_l(\epsilon)\delta_l(\epsilon)]}{\tau_l(\epsilon)} + \left(-\frac{\tau_l^{\diamond_\propto}(\epsilon)}{\tau_l(\epsilon)\tau_l^{\rho}(\epsilon)}\right)\int_{\rho(\epsilon)}^{\epsilon}\tau_l(t)\Lambda_l(t)\delta_l(t) \diamond_\propto t$$

$$= \Lambda_l(\epsilon)\delta_l(\epsilon) - \frac{\tau_l^{\diamond_\propto}(\epsilon)B_l^{\rho}(\epsilon)}{\tau_l(\epsilon)} \geq 0.$$

Applying (4) for $b \in [\rho(\epsilon), \epsilon]$, we obtain the following equality

$$\left(B_l^{\frac{\varphi_l}{y_l}}(\epsilon)\right)^{\diamond_\propto} = \frac{\varphi_l B_l^{\frac{\varphi_l}{y_l}-1}(b)}{y_l}B_l^{\diamond_\propto}(\epsilon).$$

From $B_l^{\diamond_\propto}(\epsilon) \geq 0$ and $\rho(\epsilon) \geq b$, we obtain the following inequality

$$\left(\frac{\varphi_l}{B_l^{y_l}(\epsilon)}\right)^{\diamond_\alpha} \leq \frac{\varphi_l B_l^{\left(\frac{\varphi_l}{y_l}-1\right)\rho}(\epsilon)}{y_l}\left[\Lambda_l(\epsilon)\delta_l(\epsilon) - \frac{\tau_l^{\diamond_\alpha}(\epsilon)B_l^{\rho}(\epsilon)}{\tau_l(\epsilon)}\right]$$

$$= \frac{\varphi_l \Lambda_l(\epsilon)\delta_l(\epsilon)B_l^{\left(\frac{\varphi_l}{y_l}-1\right)\rho}(\epsilon)}{y_l} - \frac{\varphi_l \tau_l^{\diamond_\alpha}(\epsilon)B_l^{\frac{\varphi_l}{y_l}\rho}(\epsilon)}{y_l \tau_l(\epsilon)}.$$

From here, we obtain the following inequality

$$\left(h_l(\epsilon)B_l^{\frac{\varphi_l}{y_l}}(\epsilon)\right)^{\diamond_\alpha} = B_l^{\frac{\varphi_l}{y_l}}(\epsilon)h_l^{\diamond_\alpha}(\epsilon) + \left(B_l^{\frac{\varphi_l}{y_l}}(\epsilon)\right)^{\diamond_\alpha} h_l^{\rho}(\epsilon)$$

$$\leq B_l^{\frac{\varphi_l}{y_l}\rho}(\epsilon)h_l^{\diamond_\alpha}(\epsilon) + \frac{\varphi_l h_l^{\rho}(\epsilon)\Lambda_l(\epsilon)\delta_l(\epsilon)B_l^{\left(\frac{\varphi_l}{y_l}-1\right)\rho}(\epsilon)}{y_l} - \frac{\varphi_l h_l^{\rho}(\varepsilon)\tau_l^{\diamond_\alpha}(\epsilon)B_l^{\frac{\varphi_l}{y_l}\rho}(\epsilon)}{y_l \tau_l(\epsilon)}. \quad (13)$$

Substituting (13) into (12), we have the following inequality

$$\int_r^\infty \frac{h_l^{\rho}(\varepsilon)\Lambda_l(\epsilon)B_l^{\frac{\varphi_l}{y_l}\rho}(\epsilon)}{\left(\Pi_{l,c}^{\rho}\Lambda(\epsilon)\right)^{\frac{\vartheta_l}{y_l}}} \diamond_\alpha \epsilon \leq \frac{y_l}{\vartheta_l - y_l}\int_r^\infty \left(\Pi_{l,c}\Lambda(\epsilon)\right)^{1-\frac{\vartheta_l}{y_l}} h_l^{\diamond_\alpha}(\epsilon)B_l^{\frac{\varphi_l}{y_l}\rho}(\epsilon) \diamond_\alpha \epsilon$$

$$+ \frac{\varphi_l}{\vartheta_l - y_l}\int_r^\infty \left(\Pi_{l,c}\Lambda(\epsilon)\right)^{1-\frac{\vartheta_l}{y_l}} h_l^{\rho}(\varepsilon)\Lambda_l(\epsilon)\delta_l(\epsilon)B_l^{\left(\frac{\varphi_l}{y_l}-1\right)\rho}(\epsilon) \diamond_\alpha \epsilon$$

$$- \frac{\varphi_l}{\vartheta_l - y_l}\int_r^\infty \frac{h_l^{\rho}(\epsilon)\tau_l^{\diamond_\alpha}(\epsilon)}{\tau_l(\epsilon)}\left(\Pi_{l,c}\Lambda(\epsilon)\right)^{1-\frac{\vartheta_l}{y_l}} B_l^{\frac{\varphi_l}{y_l}\rho}(\epsilon) \diamond_\alpha \epsilon. \quad (14)$$

From (14) and (8), we obtain the following inequality

$$\int_a^\infty \frac{h_l^{\rho}(\epsilon)\Lambda_l(\epsilon)}{\left(\Pi_{l,c}^{\rho}\Lambda(\epsilon)\right)^{\frac{\vartheta_l}{y_l}}} B_l^{\frac{\varphi_l}{y_l}\rho}(\epsilon) \diamond_\alpha \epsilon$$

$$\leq \frac{\Phi_l \varphi_l}{\vartheta_l - y_l}\int_r^\infty \left(\Pi_{l,c}\Lambda(\epsilon)\right)^{1-\frac{\vartheta_l}{y_l}} h_l^{\rho}(\epsilon)\Lambda_l(\epsilon)\delta_l(\epsilon)B_l^{\left(\frac{\varphi_l}{y_l}-1\right)\rho}(\epsilon) \diamond_\alpha \epsilon$$

$$= \frac{\Phi_l \varphi_l}{\vartheta_l - y_l}\int_r^\infty \left(\frac{\left(\Pi_{l,c}\Lambda(\epsilon)\right)^{1-\frac{\vartheta_l}{y_l}} h_l^{\rho}(\epsilon)\Lambda_l(\epsilon)\delta_l^{\frac{\varphi_l}{y_l}}(\epsilon)}{\left(\Pi_{l,c}^{\rho}\Lambda(\epsilon)\right)^{-\frac{\vartheta_l}{y_l}\left(\frac{\varphi_l}{y_l}-1\right)}}\right)^{\frac{y_l}{\varphi_l}} \times \left(\frac{h_l^{\rho}(\epsilon)\Lambda_l(\epsilon)B_l^{\frac{\varphi_l}{y_l}\rho}(\epsilon)}{\left(\Pi_{l,c}^{\rho}\Lambda(\epsilon)\right)^{\frac{\vartheta_l}{y_l}}}\right)^{\frac{\varphi_l - y_l}{\varphi_l}} \diamond_\alpha \epsilon.$$

Applying Hölder's inequality (6), we obtain the following inequality

$$\int_r^\infty \frac{h_l^{\rho}(\epsilon)\Lambda_l(\epsilon)B_l^{\frac{\varphi_l}{y_l}\rho}(\epsilon)}{\left(\Pi_{l,c}^{\rho}\Lambda(\epsilon)\right)^{\frac{\vartheta_l}{y_l}}} \diamond_\alpha \epsilon$$

$$\leq \frac{\Phi_l \varphi_l}{\vartheta_l - y_l}\left(\int_r^{\infty} \frac{\left(\Pi_{l,c}\Lambda(\epsilon)\right)^{1-\frac{\vartheta_l}{y_l}} h_l^{\rho}(\epsilon)\Lambda_l(\epsilon)\delta_l^{\frac{\varphi_l}{y_l}}(\epsilon)}{\left(\Pi_{l,c}^{\rho}\Lambda(\epsilon)\right)^{-\frac{\vartheta_l}{y_l}\left(\frac{\varphi_l}{y_l}-1\right)}} \diamond_{\propto} \epsilon\right)^{\frac{y_l}{\varphi_l}}$$

$$\times \left(\int_r^{\infty} \frac{h_l^{\rho}(\epsilon)\Lambda_l(\epsilon)\delta_l^{\frac{\varphi_l}{y_l}}(\epsilon)}{\left(\Pi_{l,c}^{\rho}\Lambda(\epsilon)\right)^{\frac{\vartheta_l}{y_l}}} \diamond_{\propto} \epsilon\right)^{\frac{\varphi_l - y_l}{\varphi_l}}.$$

From here, we obtain the following inequality

$$\int_r^{\infty} \frac{h_l^{\rho}(\epsilon)\Lambda_l(\epsilon)\delta_l^{\frac{\varphi_l}{y_l}}(\epsilon)}{\left(\Pi_{l,c}^{\rho}\Lambda(\epsilon)\right)^{\frac{\vartheta_l}{y_l}}} \diamond_{\propto} \epsilon$$

$$\leq \left(\frac{\Phi_l \varphi_l}{\vartheta_l - y_l}\right)^{\frac{\varphi_l}{y_l}} \int_r^{\infty} \frac{h_l^{\rho}(\epsilon)\Lambda_l(\epsilon)\delta_l^{\frac{\varphi_l}{y_l}}(\epsilon)\left(\Pi_{l,c}^{\rho}\Lambda(\epsilon)\right)^{\frac{\vartheta_l}{y_l}\left(\frac{\varphi_l}{y_l}-1\right)}}{\left(\Pi_{l,c}^{\rho}\Lambda(\epsilon)\right)^{\frac{\vartheta_l}{y_l}\left(\frac{\varphi_l}{y_l}-1\right)}} \diamond_{\propto} \varepsilon.$$

For $A_l > 0$, and using inequality (7), we obtain the following inequality

$$\prod_{l=1}^{m}\left(\frac{h_l^{\rho}(\epsilon)\Lambda_l(\epsilon)\left(B_l^{\rho}(\epsilon)\right)^{\varphi_l}}{\left(\Pi_{l,c}^{\rho}\Lambda(\epsilon)\right)^{\vartheta_l}}\right) = \prod_{l=1}^{m}\frac{1}{A_l^{\varphi_l}}\left\{\left(A_l \frac{B_l^{\rho}(\epsilon)\left[h_l^{\rho}(\epsilon)\Lambda_l(\epsilon)\right]^{\frac{y_l}{\varphi_l}}}{\left(\Pi_{l,c}^{\rho}\Lambda(\epsilon)\right)^{\frac{\vartheta_l}{y_l}}}\right)^{\frac{y_l}{\varphi_l}}\right\}^{y_l}$$

$$= \left[\prod_{l=1}^{m}\frac{1}{A_l^{\varphi_l}}\right]\prod_{l=1}^{m}\left\{\left(A_l \frac{B_l^{\rho}(\epsilon)\left[h_l^{\rho}(\epsilon)\Lambda_l(\epsilon)\right]^{\frac{y_l}{\varphi_l}}}{\left(\Pi_{l,c}^{\rho}\Lambda(\epsilon)\right)^{\frac{\vartheta_l}{y_l}}}\right)^{\frac{y_l}{\varphi_l}}\right\}^{y_l}.$$

Hereby

$$\int_r^{\infty}\prod_{l=1}^{m}\left(\frac{h_l^{\rho}(\epsilon)\Lambda_l(\epsilon)\left(B_l^{\rho}(\epsilon)\right)^{\varphi_l}}{\left(\Pi_{l,c}^{\rho}\Lambda(\epsilon)\right)^{\vartheta_l}}\right) \diamond_{\propto} \epsilon$$

$$\leq \left[\prod_{l=1}^{m}\frac{1}{A_l^{\varphi_l}}\right]\sum_{l=1}^{m} y_l A_l^{\frac{\varphi_l}{y_l}} \int_r^{\infty} \frac{h_l^{\rho}(\epsilon)\Lambda_l(\epsilon)\left(B_l^{\rho}(\epsilon)\right)^{\frac{\varphi_l}{y_l}}}{\left(\Pi_{l,c}^{\rho}\Lambda(\epsilon)\right)^{\frac{\vartheta_l}{y_l}}} \diamond_{\propto} \epsilon$$

$$\leq \left[\prod_{l=1}^{m}\frac{1}{A_l^{\varphi_l}}\right]\sum_{l=1}^{m} C_l \int_r^{\infty} h_l^{\rho}(\epsilon)\Lambda_l(\epsilon)\delta_l^{\frac{\varphi_l}{y_l}}(\epsilon)\frac{\left(\Pi_{l,c}^{\rho}\Lambda(\epsilon)\right)^{\frac{\vartheta_l}{y_l}\left(\frac{\varphi_l}{y_l}-1\right)}}{\left(\Pi_{l,c}^{\rho}\Lambda(\epsilon)\right)^{\frac{\varphi_l}{y_l}\left(\frac{\vartheta_l}{y_l}-1\right)}} \diamond_{\propto} \epsilon,$$

where $C_l = y_l\left(\frac{\Phi_l \varphi_l A_l}{\vartheta_l - y_l}\right)^{\frac{\varphi_l}{y_l}}$.

3. Conclusion

In this study, we establish generalizations of several existing results on fractional diamond-alpha integral inequalities by employing an alternative methodological approach. The results obtained provide a broader theoretical framework that may contribute to the investigation of mathematical problems arising in various disciplines, including mathematics, business, economics, physics, and optics. Furthermore, the diamond-alpha calculus on time scales developed in this study offers potential avenues for further generalization within the framework of alpha-conformable calculus.

References

[1] Hardy, G.H. (1920). Note on a theorem of Hilbert, Math. Z. 6(3–4), 314–317

[2] Hardy, G.H.(1925). Notes on some points in the integral calculus, LX. An inequality between integrals, Mess. Math. 54,150–156.

[3] Hardy, G.H., Littlewood, J.E. (1927). Elementary theorems concerning power series with positive coefficients and moment constants of positive functions, J. Reine Angew. Math. 157, 141–158.

[4] Hardy, G.H. (1928). Notes on some points in the integral calculus, LXIV. Mess. Math. 57, 12–16.

[5] Hardy, G.H., Littlewood, J.E., Polya, G. (1952). Inequalities Cambridge Univ; Cambridge University Press: Cambridge, UK.

[6] Akın, L. (2025). Some Innovations for Hardy-type Inequalities on Time Scales. Boletim da Sociedade Paranaense de Matemática, 43(2025), 1-11.

[7] Akın L., Zeren, Y. (2023). On innovations of the multivariable fractional Hardy-type inequalities on time scales. Sigma J Eng Nat Sci. 41(2):415−422.

[8] Akin, L., Orhan, H. (2026) New Developments of Dynamic Inequalities on Time Scales. Ukr. Math J 78, 27(2026).

[9] Akın, L., Zeren, Y. (2019). Some properties for higher order commutators of Hardy-type integral operator on Herz–Morrey spaces with variable exponent, Sigma J. Eng. & Nat. Sci.. 10(2), 157-163.

[10] Akın, L. (2018). A Characterization of Approximation of Hardy Operators in VLS, Celal Bayar University Journal of Science.14(3), 333-336.

[11] Yang, B., Rassias, M.T., Raigorodskii, A. (2021). On an extension of a Hardy–Hilbert-type inequality with multi-parameters. Mathematics, 9, 2432.

[12] Akın, L. and Samraiz, M. (2025). On Innovative Conditions of Diamond-$\propto$ Inequalities and Their Applications. Mathematical Logic Quarterly 71, no. 4 (2025): e70007. https://doi.org/10.1002/malq.70007.

[13] Akın, L. (2021). New Principles of Non-Linear Integral Inequalities on Time Scales. Applied Mathematics and Nonlinear Sciences, 6(2) 387–394.

[14] Yang, B., Wu, S., Chen, Q. (2020) A new extension of Hardy-Hilbert's inequality containing kernel of double power functions. Mathematics, 8, 894.

[15] Akın, L. and Dinç, Y. (2025) On Innovative Conditions for Weighted Hardy-Type Inequalities on Time Scales," Mathematical Methods in the Applied Sciences (2025): 16365–16374.

[16] Agarwal, R., O'Regan, D., Saker, S. (2014). Dynamic Inequalities on Time Scales; Springer: Cham, Switzerland.

[17] Akin-Bohner, E., Bohner, M., Akin, F. (2005) Pachpatte inequalities on time scales. JIPAM J. Inequal. Pure Appl. Math., 6, 6.

[18] Bohner, M., Matthews, T. (2007) The Grüss inequality on time scales. Commun. Math. Anal., 3, 1–8.

[19] Bohner, M., Matthews, T. (2008). Ostrowski inequalities on time scales. JIPAM J. Inequal. Pure Appl. Math., 9, 8.

[20] Dinu, C. (2008). Hermite-Hadamard inequality on time scales. J. Inequal. Appl., 2008, 287947.

[21] Cheung, W.-S., Hanjs, Z., Pecari´c, J. (2000). Some Hardy-type inequalities. *J. Math. Anal. Appl*. 250, 621–634.

[22] Hilscher, R. (2002) A time scales version of a Wirtinger-type inequality and applications. J. Comput. Appl. Math., 141, 219–226.

[23] Li, W.N. (2010). Some delay integral inequalities on time scales. Comput. Math. Appl., 59, 1929–1936.

[24] Rehák, P. (2005). Hardy inequality on time scales and its application to half-linear dynamic equations. J. Inequal. Appl., 2005, 942973.

[25] Hilger, S. (1988) Ein Maßkettenkalkül mit Anwendung auf Zentrumsmannigfaltigkeiten. Ph.D. Thesis, Universität Würzburg, Würzburg, Germany.

[26] Rahmat, M.R.S., Noorani, M.S.M. (2021) A new conformable nabla derivative and its application on arbitrary time scales. Adv. Differ. Equ., 2021, 238.

[27] Mamedov, F.I., Zeren, Y., Akın, L. (2017). Compactification of

weighted Hardy operator in variable exponent Lebesgue spaces, Asian Journal of Mathematics and Computer Science. 17(1), 38-47

[28] Hilger, S. (1990). Analysis on measure chains-a unified approach to continuous and discrete calculus, Results Maths. 18(1-2) 18–56.

[29] Ahmad, W., Khan, K.A., Nosheen, A., Sultan, M.A. (2019). Copson, Leindler-type inequalities for functions of several variables on time scales, Punjab Univ. J. of Math. 51(8),157–168.

[30] Ashraf, M.S., Khan, K.A., Nosheen, A. (2019). Hardy-Copson type inequalities on time scales for the functions of n independent variables, Int. J. Anal. Appl. 17(2), 244–259.

[31] Baric, J., Bibi, R., Bohner, M., Nosheen, A., Pecaric, J. (2015). Jensen inequalities and their applications on time scales, Element, Zagreb, Croatia

[32] Akın, L. (2024). On Some Inequalities for Exponentially Weighted Fractional Hardy Operators with Δ-Integral Calculus. Middle East Journal of Science, Vol. 10, No. 1, pp. 1–13, 2024, doi: 10.51477/mejs.1451041.

[33] Saker, S.H., O'Regan, D. (2016) Hardy and Littlewood Inequalities on time scales, Bull. Malays. Math. Sci. Soc. 39(2) 527–543.

[34] Li, W., Liu, D., Liu, J. (2019). Weighted inequalities for fractional Hardy operators and commutators, Journal of Inequalities and Applications 2019:158, 1-14.

[35] Bradley, J. (1978). Hardy inequalities with mixed norms. Can. Math. Bull. 21(4), 405-408.

[36] Kufner, A., Persson, L.E. (2003). Weighted Inequalities of Hardy Type. World Scientific, Singapore.

[37] Opic, B., Kufner, A. (1990). Hardy-Type Inequalities. Pitman Research Notes in Mathematics Series, Longman Scientific and Technical, Harlow, Essex.

[38] Akın, L. (2020). On some results of weighted Hölder type inequality on time scales. Middle East Journal of Science 6(1), 15-22.

[39] Akın L.(2021). On innovations of n-dimensional integral-type inequality on time scales. Adv. Differ. Equ. 2021:148.

[40] Bohner, M., Nosheen, A., Pecaric, J., Younas, A. (2014). Some dynamic Hardy-type inequalities on time scales, J. Math. Inequal. 8(1), 185–199.

[41] Agarwal, R.P., Bohner, M., O'Regan, D., Saker, S.H. (2011). Some Wirtinger-type inequalities on time scales and their applications, Pacific J. Math. 252, 1–26 (2011)

[42] Akın, L. (2020). On the Fractional Maximal Delta Integral Type Inequalities on Time Scales. Fractal Fract. 4, 26, 1-10.

[43] Bohner, M., Peterson, A. (2001). Dynamic Equations on Time Scales. An Introduction with Applications, Birkhauser, Boston.

[44] Akın L. (2021). A New Approach for the Fractional Integral Operator in Time Scales with Variable Exponent Lebesgue Spaces. Fractal Fract. 5(7), 1-13.

[45] Bohner, M., Georgiev, S.G. (2016). Sequences and Series of Functions. In: Multivariable Dynamic Calculus on Time Scales, Springer Int. Publ. Switzerland.

[46] Akın, L. (2024). On generalized weighted dynamic inequalities for diamond-$\propto$ integral on time scales calculus. Indian J Pure Appl Math 55, 363–376.

[47] Anastassiou, G.A. Principles of delta fractional calculus on time scales and inequalities. Math. Comput. Model. 2010, 52, 556–566.

[48] Saker, S.H., El-Sheikh, M.M.A., Madian, A.M. (2021) Some new generalized weighted dynamic inequalities of Hardy's type on time scales, J. Math. Computer Sci., 23 (2021), 289–301.

[49] Almarri, B., El-Deeb, A.A. (2023) Gamma-Nabla Hardy–Hilbert-Type Inequalities on Time Scales. Axioms, 12, 449.

[50] Tejado, I., Valerio, D., Valerio, N. (2015) Fractional Calculus in Economic Growth Modelling: the Spanish Case. Netherlands: Springer.

[51] Güvenilir, A.F., Kaymakçalan, B., Pelen, N.N.(2015) Constantin's inequality for nabla and diamond alpha derivative. J. Inequal. Appl. 2015(167), 1–17.

[52] Kac, V., Cheung, P. (2002). Quantum Calculus. Universitext Springer, New York.

[53] Bohner, M., Agarwal, R.P. (1999). Basic calculus on time scales and some of its applications, Resultate der Mathematik. 35, 3- 22.

[54] Agarwal, R.P., O'Regan, D., Saker, S.H. (2016). Hardy Type Inequalities on Time Scales, Springer, Switzerland.

CHAPTER 2

Nonlinear Diffusion Equations: Mathematical Foundations and Numerical Experiments

Özlem Kaytmaz[1]

[1] Assoc. Prof. Dr., Zonguldak Bülent Ecevit University, Faculty of Science, Department of Mathematics, Division of Applied Mathematics, ORCID: 0000-0003-0420-007X

1. Introduction

Diffusion equations are among the basic partial differential equation models used to describe the temporal evolution of a quantity distributed in space. The classical heat equation represents linear spreading with a constant diffusion coefficient and is one of the standard models in the theory of parabolic equations. In many mathematical models, however, the rate of spreading is not constant; it may depend on the magnitude of the solution, the density, or another state variable. This leads naturally to nonlinear diffusion equations. Their importance stems not only from the range of applications they represent, but also from qualitative features that differ markedly from those of the linear theory (Kalashnikov, 1987; Vázquez, 2007).

In one space dimension, the classical model with constant diffusion coefficient can be written as

$$\frac{\partial u}{\partial t} = D\frac{\partial^2 u}{\partial x^2}, \quad D > 0 \tag{1}$$

Here $u = u(x,t)$ denotes the diffusing quantity, whereas D is the constant diffusion coefficient. If the diffusion coefficient is allowed to depend on the solution, the more general nonlinear form

$$\frac{\partial u}{\partial t} = \nabla \cdot (D(u)\nabla u) \tag{2}$$

is obtained. The resulting flux relation is then nonlinear because the diffusion coefficient depends on the solution. If the diffusion coefficient approaches or attains zero for some solution values, uniform parabolicity may be lost, leading to a degenerate diffusion equation.

A canonical model within this class is the porous medium equation (PME),

$$\frac{\partial u}{\partial t} = \Delta(u^m), \quad m > 1 \tag{3}$$

By the chain rule, the effective diffusion coefficient in this equation depends on a power of the solution. In particular, its vanishing as the solution approaches zero is the principal degeneracy mechanism of the PME. This feature is closely associated with finite propagation, preservation of compact support, and a moving free boundary, none of which occurs in the same form for the classical heat equation (Vázquez, 1992, 2007).

For the linear heat equation with nontrivial nonnegative compactly supported initial data, the solution becomes positive throughout space at every positive time. For the PME, by contrast, the support of suitable compactly supported data expands at a finite rate. The boundary of the positivity set therefore becomes a moving interface. This distinction is important both analytically and computationally. On a fixed grid, the moving interface does not in general

coincide with grid points, and the numerical error may consequently behave differently near the edge of the support.

Another central feature of the PME is its family of self-similar solutions. Barenblatt-type solutions display, in a single explicit formula, the decay of the amplitude and the expansion of compact support. These solutions also play an important role in the analysis of long-time behavior and convergence toward self-similarity (Carrillo & Toscani, 2000; Vázquez, 2007). Their explicit form provides a convenient reference profile for numerical assessment (Barenblatt, 1953; Vázquez, 2007).

For degenerate parabolic equations, accuracy alone does not provide a complete assessment of a numerical approximation. It is also important to avoid spurious negative values for nonnegative data, to preserve total mass under appropriate boundary conditions, to represent the moving support adequately, and to limit artificial numerical diffusion near the moving interface. Accordingly, finite-difference, finite-volume, and structure-preserving discretizations have been extensively studied for nonlinear and degenerate diffusion problems (Bessemoulin-Chatard & Filbet, 2012; Chainais-Hillairet et al., 2016; Eymard et al., 2002; Liu et al., 2011).

This chapter examines the fundamental mathematical properties of nonlinear diffusion equations through the porous medium equation as a representative degenerate model. The conservation and degeneracy structures are first described, followed by an analysis of finite propagation, compact support, moving interfaces, and self-similar behavior. An explicit conservative finite-difference approximation is then employed for the numerical solution of the one-dimensional problem. The numerical approximation is assessed against a Barenblatt reference solution using discrete error norms and mesh-refinement analysis. Finally, computations performed for several nonlinear exponents are used to examine their influence on the computed solution profiles and spatial spreading.

2. Mathematical Foundations of Nonlinear Diffusion Equations

2.1. Diffusive Flux and Conservation Structure

A nonlinear diffusion problem defined in a domain Ω can be written in the general form

$$u_t = \nabla \cdot (D(u)\nabla u), (x,t) \in \Omega \times (0,T] \quad (4)$$

When the equation is written as a conservation law,

$$u_t + \nabla \cdot J = 0 \quad (5)$$

with the nonlinear Fick-type flux

$$J = -D(u)\nabla u \quad (6)$$

is obtained. Thus, the local variation of the solution is governed by the divergence of the flux. If the effective diffusion coefficient admits a positive lower bound over the relevant range of solution values, namely

$$D(u) \geq D_0 > 0 \tag{7}$$

the degeneracy associated with a vanishing diffusion coefficient is avoided. Degeneracy occurs when the coefficient $D(u)$ approaches or attains zero for some solution values. Nonlinear diffusion equations are also frequently written as

$$u_t = \Delta \Phi(u) \tag{8}$$

where

$$\Phi'(u) = D(u) \tag{9}$$

This representation is particularly convenient in the study of monotonicity, weak solutions, and energy or entropy structures (Kalashnikov, 1987; Vázquez, 2007).

2.2. Power-Law Diffusion and Degeneracy

For a power-law nonlinearity, let

$$\Phi(u) = u^m \tag{10}$$

and hence

$$D(u) = m\, u^{m-1} \tag{11}$$

With this choice, the general diffusion equation reduces to

$$u_t = \Delta(u^m) \tag{12}$$

The case $m = 1$ gives the classical heat equation, whereas the porous medium regime corresponds to m>1. For positive solutions, the behavior of the effective diffusion coefficient near zero is described by

$$\lim_{u \to 0^+} m\, u^{m-1} = 0, \quad m > 1 \tag{13}$$

This limit shows that diffusion weakens in regions where the solution is small. The equation is therefore nondegenerate within the positivity set but becomes degenerate at its boundary. This mechanism underlies the finite speed of propagation.

2.3. Initial-Boundary Value Problem and Mass

In one space dimension, on the interval Ω=(a,b), an initial-boundary value problem may be written as

$$u_t = \frac{\partial}{\partial x}(D(u)u_x), \quad a < x < b, \quad 0 < t \leq T \tag{14}$$

together with the initial condition

$$u(x,0) = u_0(x) \tag{15}$$

A homogeneous Dirichlet condition may be prescribed as

$$u(a,t) = u(b,t) = 0 \tag{16}$$

For mass conservation, the natural boundary condition is the zero-flux condition

$$D(u)u_{\mathrm{x}}(a,t) = D(u)u_{\mathrm{x}}(b,t) = 0 \tag{17}$$

The total mass of the solution is defined by

$$M(t) = \int_a^b u(x,t)\,dx \tag{18}$$

Integrating the equation with respect to the spatial variable gives

$$\frac{dM}{dt} = [D(u)u_x]_a^b \tag{19}$$

Under zero flux, the boundary terms vanish and

$$M(t) = M(0) \tag{20}$$

This conservation property provides a basic quantitative diagnostic for the numerical solution.

2.4. Nonnegativity and the Weak-Solution Perspective

The PME is usually considered with nonnegative initial data:

$$u_0(x) \geq 0 \tag{21}$$

Because of degeneracy, classical derivatives need not retain sufficient regularity across the interface. General existence and uniqueness results, together with qualitative properties, are therefore established within a weak or generalized solution framework. Kalashnikov (1987) provides a broad account of the

qualitative theory of degenerate second-order parabolic equations, while Vázquez (2007) develops the solution theory, finite propagation, and asymptotic behavior of the porous medium equation in a systematic form. Here we use only those structural properties that are directly relevant to the subsequent numerical analysis.

3. A Fundamental Model of Nonlinear Diffusion: The Porous Medium Equation

Among nonlinear diffusion equations, the porous medium equation is a canonical model in which degeneracy and finite propagation appear explicitly. In d-dimensional space, the equation is

$$u_t = \Delta(u^m), \quad m > 1 \tag{22}$$

In one dimension, it becomes

$$u_t = (u^m)_{xx} \tag{23}$$

with initial data

$$u(x,0) = u_0(x) \geq 0 \tag{24}$$

The nonlinearity influences not only the amplitude of the solution but also the geometry and temporal evolution of its positivity set (Vázquez, 1992, 2007).

3.1. Finite Propagation and Compact Support

For a fixed time t, define the positivity set by

$$P(t) = \{x \in \mathbb{R} : u(x,t) > 0\} \tag{25}$$

If the initial support

$$\text{supp } u_0 = \overline{P(0)} \tag{26}$$

is compact, then under suitable assumptions the support of a PME solution remains bounded at every finite time. This is a fundamental departure from the infinite propagation speed of the classical heat equation. Finite propagation creates a moving boundary between the zero and positive regions of the solution. Since the location of this boundary is determined together with the solution, the problem has a free-boundary character.

3.2. Moving Interface

In one dimension, when the positivity set is a single interval, it may be represented as

$$P(t) = (s_{-}(t), s_{+}(t)) \tag{27}$$

where the endpoints represent the moving interfaces. With a fixed-grid discretization, these interfaces are not expected to coincide exactly with grid points. The maximum-norm error may therefore be sensitive to the location of the interface relative to the grid. Mesh-refinement results can consequently reflect not only the magnitude of the discretization error but also small variations associated with the discrete representation of the moving boundary.

3.3. Conservation of Mass

On the whole real line, under sufficient decay at infinity, the total mass is defined by

$$M(t) = \int \mathbb{R}\, u(x,t)\, dx \tag{28}$$

and satisfies

$$M(t) = M(0) \tag{29}$$

Formally,

$$\frac{d}{dt}\int_{\mathbb{R}} u\, dx = \int_{\mathbb{R}} (u^m)_{xx}\, dx \tag{30}$$

and mass conservation follows when the boundary fluxes vanish. Monitoring the discrete mass in numerical experiments is therefore useful for assessing how faithfully the computation reflects the conservation structure.

3.4. Role of the Nonlinear Exponent

For the PME, the effective diffusion coefficient is

$$D(u) = m\, u^{m-1} \tag{31}$$

so the parameter m directly changes the diffusion mechanism. In the limit $m = 1$,

$$u_t = \Delta u \tag{32}$$

the linear heat equation is recovered. For $m>1$, the effective diffusivity vanishes as u approaches zero, producing degeneracy near the interface. In particular, as u approaches zero, increasing m causes $u^{m-1}$to decay more rapidly, thereby strengthening the degeneracy near the interface. In the numerical experiments below, the influence of this parameter is compared through the maximum value

$$u_{\max}(t) = \max_x u(x,t) \tag{33}$$

the total mass, and the effective support width.

3.5. An Energy-Dissipation Property

For sufficiently smooth solutions and suitable boundary behavior, the one-dimensional PME satisfies a simple energy/entropy-type dissipation relation. Multiplying the equation by the indicated power of the solution and integrating in space gives

$$\int u^m u_t \, dx = \int u^m (u^m)_{xx} \, dx \tag{34}$$

The left-hand side can be written as

$$\frac{1}{m+1}\frac{d}{dt}\int u^{m+1} \, dx \tag{35}$$

while integration by parts on the right-hand side yields

$$\int u^m (u^m)_{xx} \, dx = -\int |(u^m)_x|^2 \, dx \tag{36}$$

Consequently,

$$\frac{d}{dt}\left[\frac{1}{m+1}\int u^{m+1} \, dx\right] = -\int |(u^m)_x|^2 dx \leq 0 \tag{37}$$

Such dissipation structures are important both for understanding the long-time behavior of nonlinear diffusion and for constructing discretizations that reproduce energy or entropy properties at the discrete level (Carrillo et al., 2001; Chainais-Hillairet et al., 2016; Otto, 2001).

4. Self-Similar and Barenblatt-Type Solutions

Self-similar solutions form one of the fundamental solution families of the PME. In d dimensions, consider

$$u_t = \Delta(u^m), \quad m > 1 \tag{38}$$

and introduce an ansatz of the form

$$u(x,t) = t^{-\alpha} F(\eta), \quad \eta = |x| \, t^{-\beta} \tag{39}$$

Comparison of the scaling of the time derivative and the diffusion term gives

$$\alpha + 1 = \alpha m + 2\beta \tag{40}$$

The total mass is

$$M = \int_{\mathbb{R}^d} u(x,t)\, dx \tag{41}$$

and the change of variables contributes a factor $t^{-\alpha+d\beta}$. Requiring the mass to be independent of time gives

$$\alpha = d\beta \tag{42}$$

Solving these two relations yields

$$\alpha = \frac{d}{d(m-1)+2}, \qquad \beta = \frac{1}{d(m-1)+2} \tag{43}$$

In particular, in one space dimension,

$$\alpha = \beta = \frac{1}{m+1} \tag{44}$$

This scaling displays explicitly the balance between decay of the solution amplitude and expansion of its support.

4.1. Barenblatt Profile

The classical Barenblatt-type self-similar profile for the PME can be written as

$$U(x,t) = t^{-\alpha}\left[C - k|x|^2 t^{-2\beta}\right]_+^{\frac{1}{m-1}} \tag{45}$$

where the positive-part function is

$$(s)_+ = \max\{s, 0\} \tag{46}$$

and the coefficient is

$$k = \frac{\beta(m-1)}{2m} \tag{47}$$

In one dimension, using $\alpha=\beta=\frac{1}{m+1}$ gives

$$U(x,t) = t^{-\frac{1}{m+1}}\left[C - \frac{m-1}{2m(m+1)}\, x^2\, t^{-\frac{2}{m+1}}\right]_+^{\frac{1}{m-1}} \tag{48}$$

The resulting Barenblatt profile (Barenblatt, 1953; Vázquez, 2007) is positive precisely where the expression in brackets is positive. Hence the support radius is

$$R(t) = \sqrt{\frac{C}{k}}\, t^{\beta} \tag{49}$$

and the support is

$$\text{supp U}(\cdot, \text{t}) \;=\; [-\text{R(t)}, \text{R(t)}] \tag{50}$$

The maximum value at the center is

$$U(0,t) = C^{\frac{1}{m-1}} t^{-\frac{1}{m+1}} \tag{51}$$

Thus the amplitude decays at the rate $t^{-\alpha}$, whereas the support radius grows at the rate t^{β}. In one dimension, both scaling exponents are $\frac{1}{m+1}$.

4.2. Role in Numerical Assessment

Because the Barenblatt profile is known explicitly, it can be used as a reference solution for numerical assessment. At the final time T, the discrete L^2 and maximum-norm errors are defined, respectively, by

$$E_2 \;=\; \left[h \sum_i |{u_i}^M \;-\; U(x_i, T)|^2 \right]^{\frac{1}{2}} \tag{52}$$

$$E_\infty \;=\; \max_i |{u_i}^M \;-\; U(x_i, T)| \tag{53}$$

The observed order of convergence based on two successive grids is computed from

$$p = \frac{\log\left(\frac{E_h}{E_{\frac{h}{2}}}\right)}{\log 2} \tag{54}$$

For degenerate problems with moving interfaces, the observed order need not vary monotonically at every refinement level. Error magnitudes, refinement trends, and profile comparisons should therefore be considered together.

5. Numerical Approximation

The numerical experiments use an explicit finite-difference approximation for the one-dimensional porous medium equation:

$$u_t = (u^m)_{xx}, \quad a < x < b, \quad 0 < t \leq T, \quad m > 1 \tag{55}$$

Let the initial condition be

$$u(x, 0) = u_0(x) \tag{56}$$

Divide the spatial interval into N equal subintervals and define

$$h = \frac{b-a}{N}, \qquad x_i = a + ih, i = 0, \dots, N \tag{57}$$

Let Δt denote the time step and ${u_i}^n$ the approximation at the time level t_n. Combining the centered spatial difference

$$(u^m)_{xx}(x_i, t_n) \approx \frac{(u_{i+1}^n)^m - 2(u_i^n)^m + (u_{i-1}^n)^m}{h^2} \tag{58}$$

with forward Euler time discretization gives the explicit scheme

$$u_i^{n+1} = u_i^n + \frac{\Delta t}{h^2}[(u_{i+1}^n)^m - 2(u_i^n)^m + (u_{i-1}^n)^m] \tag{59}$$

The method is straightforward to implement, but the time step must be chosen in accordance with the nonlinear effective diffusivity.

5.1. Discrete Conservation Form

The continuous equation may be written as

$$u_t + J_x = 0, \quad J = -(u^m)_x \tag{60}$$

If the half-node numerical flux is defined by

$$J_{i+\frac{1}{2}}^n = -\frac{(u_{i+1}^n)^m - (u_i^n)^m}{h} \tag{61}$$

the scheme takes the conservative form

$$\frac{u_i^{n+1} - u_i^n}{\Delta t} + \frac{J_{i+\frac{1}{2}}^n - J_{i-\frac{1}{2}}^n}{h} = 0 \tag{62}$$

Summation over the interior nodes causes the flux terms to cancel telescopically. When the boundary fluxes vanish, the discrete total mass

$$M_h{}^n \;=\; h \sum_i u_i{}^n \tag{63}$$

is conserved up to round-off error. In the Barenblatt reference-solution experiment, the computational interval is chosen so that the support of the reference solution remains away from the boundary; therefore, the reference solution has zero boundary flux at the computational boundary.

5.2. Time-Step Restriction and Nonnegativity

Writing the PME in the form

$$u_t \;=\; (m\, u^{m-1}\, u_x)_x \tag{64}$$

shows that the effective diffusion coefficient is

$$D(u) \;=\; m\, u^{m-1} \tag{65}$$

A conservative time-step restriction for the explicit scheme may be taken as

$$\Delta t \le \frac{\theta h^2}{m \max_i (u_i^n)^{m-1}}, \qquad 0 < \theta \le \frac{1}{2} \tag{66}$$

In the computations, at each time level we use

$$\Delta t_n = \frac{\theta h^2}{m \max_i (u_i^n)^{m-1}} \tag{67}$$

with the final step shortened when necessary to reach the prescribed final time exactly. This choice is used to control the explicit update in accordance with the nonlinear diffusivity.

5.3. Initial Data and Reference Solution

Because the Barenblatt fundamental solution has a singular initial structure at $t = 0$, the numerical assessment is started at a positive time t_0:

$$u_i{}^0 \;=\; U(x_i, t_0), \;\; t_0 \;>\; 0 \tag{68}$$

The scheme is then advanced from t_0 to T. The computational interval $[a,b]$ is chosen large enough to contain the Barenblatt support throughout the time interval, and homogeneous zero values are imposed at the endpoints. Since the

support does not reach the endpoints, this boundary treatment is consistent with the reference solution.

5.4. Error and Mesh-Refinement Analysis

At the final time level $t_M = T$, define the error by

$$e_i = u_i^M - U(x_i, T) \tag{69}$$

and compute the norms

$$E_2 = \left[h \sum_i |e_i|^2\right]^{\frac{1}{2}}, \quad E_\infty = \max_i |e_i| \tag{70}$$

The mesh-refinement study uses $N = 50, 100, 200$, and 400. The centered spatial difference is second-order accurate in smooth regions, while forward Euler is first-order accurate in time. Since the stability restriction gives $\Delta t = O(h^2)$, an overall behavior close to second order can be expected in sufficiently smooth regions. The limited regularity at the PME interface may, however, affect the observed rate. For this reason, the convergence order is computed from the numerical results rather than imposed a priori.

6. Numerical Experiments and Discussion

6.1. Assessment Against a Reference Solution

In the first experiment, $m = 2$, $C = 1$, t_0=1, and $T = 2$ are used. The computational interval is $[-6,6]$, and the time-step parameter is set to $\theta = 0.4$. With these values, the one-dimensional Barenblatt solution reduces to

$$U(x,t) = t^{-\frac{1}{3}} \left[1 - \frac{x^2}{12} t^{-\frac{2}{3}}\right]_+ \tag{71}$$

Since the support radius is $R(t) = \sqrt{12}\, t^{\frac{1}{3}}$, the support remains inside $[-6,6]$ up to $T = 2$. The boundary treatment therefore has no influence on the reference profile.

Table 1. Errors and observed mesh-refinement behavior relative to the Barenblatt reference solution

N	h	$\mathbf{E_2}$	$p(\mathbf{E_2})$	$E\infty$	$p(E\infty)$
50	0.240	0.003547	–	0.004651	–
100	0.120	0.000790	2.167	0.001037	2.165
200	0.060	0.000581	0.442	0.001521	−0.553
400	0.030	0.000080	2.865	0.000291	2.386

Source: Numerical computations performed by the author.

Table 1 shows an overall reduction in the error as the mesh is refined. At $N = 100$, both norms display behavior close to second order, whereas the transition at $N = 200$ is nonmonotone, particularly in the maximum norm. This may be related to the position of the moving interface relative to the discrete grid and to the limited regularity near the interface. It is therefore more informative to consider the entire refinement sequence than to infer an order from a single pair of successive grids. For $N = 400$, both errors decrease substantially again and the numerical profile is very close to the reference solution.

Table 2. Discrete mass values in the reference-solution experiment

N	$\mathbf{M_h}(t_0)$	$\mathbf{M_h}(T)$	$\lvert\mathbf{M_h}(T)-\mathbf{M_h}(t_0)\rvert$
50	4.621440	4.621440	8.88×10^{-16}
100	4.618368	4.618368	0
200	4.618860	4.618860	0
400	4.618845	4.618845	0

Source: Numerical computations performed by the author.

The initial and final discrete masses are reported in Table 2. Their differences are at the level of machine precision, indicating that the conservative form together with the zero boundary flux effectively preserves the discrete total mass in this experiment. As the grid is refined, the discrete initial mass becomes increasingly consistent with the integral of the continuous Barenblatt profile.

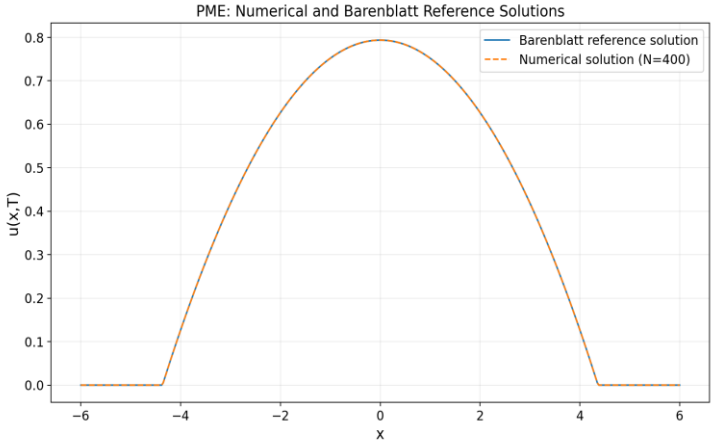


Figure 1. Comparison of the numerical and Barenblatt reference solutions for $m = 2$, $T = 2$, and $N = 400$

Source: Numerical computations performed by the author.

For the finest grid, the numerical and reference profiles in Figure 1 are almost indistinguishable. The most sensitive regions are located near the endpoints of the support, where the moving interfaces occur. This observation is consistent with the maximum-norm behavior in Table 1 and illustrates the importance of interface resolution in degenerate diffusion problems.

6.2. Effect of the Nonlinear Exponent

In the second experiment, the same initial profile is used in all computations in order to isolate the effect of the parameter m:

$$u_0(x) = [1 - x^2]_+ \tag{72}$$

The computational interval is $[-3,3]$, with $N = 400$, $T = 0.2$, and $\theta = 0.4$; the same explicit scheme is applied for $m = 2, 3\ and\ 4$. To prevent values at the level of round-off from affecting the comparison, the numerical effective support is defined as the width spanned by nodes satisfying $u_i > 10^{-6}$.

Table 3. Solution measures for different nonlinear exponents, $T = 0.2$

m	max $u(T)$	$M_h(0)$	$M_h(T)$	Mass difference	Support width
2	0.665020	1.333358	1.333358	2.22×10^{-16}	3.03
3	0.684354	1.333358	1.333358	2.22×10^{-16}	2.52
4	0.705407	1.333358	1.333358	4.44×10^{-16}	2.28

Source: Numerical computations performed by the author.

According to Table 3, as m increases, the maximum solution value at $T = 0.2$ increases while the effective support width decreases. In all three computations, which start from the same initial mass, total mass is preserved to machine precision. The differences between the profiles therefore reflect spatial redistribution by the nonlinear diffusion mechanism rather than loss of mass. As u approaches zero, increasing m causes u^{m-1} to decay more rapidly, so the effective diffusion becomes more strongly degenerate in the low-amplitude region near the interface. Over the short time interval considered here, the numerical results exhibit a narrower effective support and a higher peak as the nonlinear exponent increases.

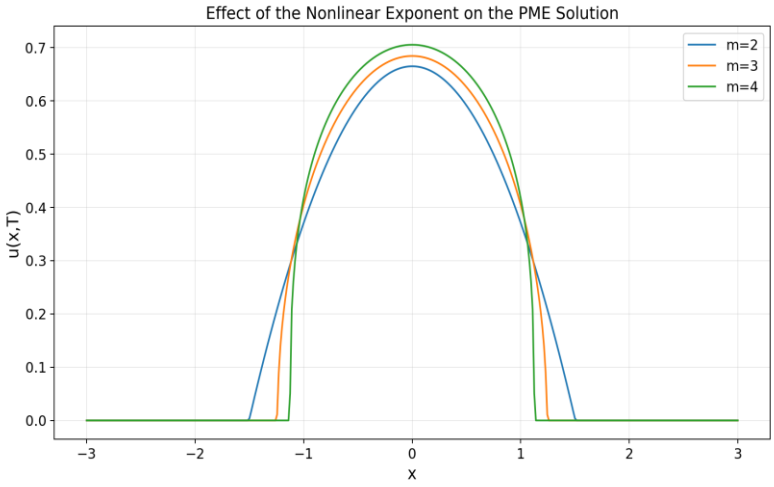


Figure 2. Numerical solution profiles at $m = 2, 3\ and\ 4$ for $T = 0.2$
Source: Numerical computations performed by the author.

Figure 2 supports these quantitative observations. The solution for $m = 2$ spreads over a wider region and has a lower central height, whereas the solution for $m = 4$ has a narrower support and a higher central value. The $m = 3$ profile lies between these two cases. Thus the nonlinear exponent influences not only the local diffusion coefficient but also the macroscopic spreading pattern of the solution.

7. Conclusion

This chapter has considered nonlinear diffusion equations from both mathematical and numerical viewpoints. Beginning with the general nonlinear diffusion structure, attention was focused on the porous medium equation as a canonical representative of the class. The main features distinguishing it from the linear heat equation—degeneracy, finite propagation, compact support, and a moving interface—were examined together with mass conservation and an energy-dissipation structure.

Self-similar solutions, in particular the Barenblatt profile, were then used to describe the characteristic behavior of the porous medium equation. The self-similar scaling captures in a unified form the decay of the amplitude and the expansion of the support. These properties also make the Barenblatt solution a natural reference profile for numerical assessment.

For the numerical study, an explicit finite-difference approximation was applied to the one-dimensional porous medium equation. The scheme was expressed in conservative form, and the time step was selected according to the nonlinear effective diffusivity. The assessment included discrete L^2 and

maximum error norms, mesh-refinement behavior, and conservation of total mass, rather than relying on graphical comparison alone.

In the Barenblatt reference-solution experiment, the overall error decreased under mesh refinement and the finest-grid solution agreed closely with the reference profile. The observed convergence order was not monotone at every refinement level, a feature that may be associated with the position of the moving interface on the discrete grid. This behavior emphasizes that interface effects should be taken into account when numerical errors are interpreted for degenerate parabolic problems.

The second experiment showed that, for a common initial profile, the parameter m has a clear influence on spatial spreading. As m increased, the maximum value became larger while the effective support width decreased. In each case, the total mass was conserved to machine precision; thus, within these computations, the observed differences between the profiles are associated with spatial redistribution under nonlinear diffusion rather than with numerical mass loss.

Taken together, the analytical properties and numerical results show why the porous medium equation remains a useful model problem for nonlinear diffusion. Further work may consider higher-order time discretizations, implicit schemes, adaptive meshes, and more accurate interface tracking. Comparisons between classical finite-difference methods and discretizations that preserve energy or entropy structures at the discrete level would also be useful for a more detailed study of long-time behavior.

CHAPTER 3

Küme Değerli Analizde Temel Tanımlar

Gonca İnceoğlu[1]

[1] Dr. Öğr. Üyesi, Anadolu Üniversitesi, Eğitim Fakültesi, Matematik ve Fen Bilimleri Eğitimi Bölümü, ORCID: 0000-0002-5237-6822

Giriş

Küme değerli analiz, bir noktaya tek bir değer yerine bir değerler kümesi karşılık getiren dönüşümlerin incelenmesini konu alır. Bu yaklaşım, çözümün veya çıktının tek bir elemanla ifade edilemediği matematiksel modeller için bir çerçeve sunar. Küme değerli dönüşümlerin grafikleri, süreklilik özellikleri ve türev kavramları bu alanın temel inceleme konuları arasındadır (Aubin ve Frankowska, 2009). Vektör ve küme değerli optimizasyonda ise değer uzayındaki sıralama yapısı, çözümlerin hangi anlamda karşılaştırılacağını belirler (Jahn, 2011).

Küme değerli dönüşümlerle çalışabilmek için lineer uzaylar, konveks kümeler, koniler ve sıralama bağıntılarının birlikte ele alınması gerekir. Normlu uzayların sağladığı yakınsama ve kapanış yapıları, contingent ve radyal konilerin tanımlanmasında kullanılır. Konvekslik, üst grafik ve subdiferansiyel kavramları ise konveks analiz ile optimizasyon arasındaki temel bağlantıları oluşturur (Rockafellar, 1970).

Reel değerli problemlerde alışılmış sayı sıralaması kullanılırken vektör değerli problemlerde karşılaştırma çoğunlukla bir koni yardımıyla yapılır. Bu nedenle en küçük eleman kavramı ile minimal eleman kavramı birbirinden ayrılır. Minimal, zayıf minimal ve Benson anlamında has minimal elemanlar, sıralama konisinin geometrisine bağlı farklı optimalite kavramlarıdır (Jahn, 2011). Bu ayrımların açık biçimde ortaya konulması, küme değerli optimizasyonun sonraki aşamalarında kullanılacak tanımların anlaşılması açısından gereklidir.

Klasik türev kavramının doğrudan uygulanamadığı durumlarda, bir kümenin veya üst grafiğin geometrisinden yararlanılır. Contingent koni, kümenin bir noktası yakınındaki teğetsel davranışını; kapalı radyal koni ise o noktadan kümeye yönelen radyal doğrultuların kapanışını betimler (Aubin ve Frankowska, 2009). Jahn ve Rauh tarafından tanımlanan contingent üst türev, küme değerli bir dönüşümün üst grafiğine ait contingent koniyi bir türev dönüşümünün üst grafiği aracılığıyla ifade eder (Jahn ve Rauh, 1997). Böylece küme geometrisi ile türev kavramı arasında bir bağlantı kurulur.

Bu bölümün amacı, küme değerli analizin temel kavramlarını ortak bir gösterim altında sunmaktır. Önce lineer uzaylar, konveks kümeler, koniler ve sıralama bağıntıları; ardından vektörel norm ve Daniell konisi ele alınmaktadır. Son kısımda dönüşümler, contingent ve kapalı radyal koniler, küme değerli dönüşümlerin grafikleri ve üst grafikleri, minimalite kavramları ile subdiferansiyel tanımı verilmektedir. Normlu uzaylara ilişkin temel topolojik kavramların bilindiği varsayılmaktadır.

Lineer Uzaylar, Konveks Kümeler ve Sıralama

Tanım 1.1: Herhangi bir X kümesi verilsin ve X kümesi üzerinde toplama ve skalerle çarpma işlemleri; yani (Jahn, 2011; Schaefer ve Wolff, 1999)

$$+: X \times X \to X$$

ve

$$\cdot : \mathbb{R} \times X \to X$$

tanımlansın.

Eğer her $x, y, z \in X$ ve her $\lambda, \mu \in \mathbb{R}$ için aşağıdaki aksiyomlar sağlanıyorsa o zaman X kümesine reel lineer uzay denir:

a) $(x + y) + z = x + (y + z)$;
b) $x + y = y + x$;
c) Bir $0_X \in X$ elemanı vardır öyle ki her $x \in X$ için $x + 0_X = x$;
d) Her $x \in X$ için bir $y \in X$ vardır öyle ki $x + y = 0_X$;
e) $\lambda(x + y) = \lambda x + \lambda y$;
f) $(\lambda + \mu)x = \lambda x + \mu x$;
g) $\lambda(\mu x) = (\lambda\mu)x$;
h) $1x = x$.

Tanım 1.2: S ve T kümeleri reel normlu X uzayının boş olmayan alt kümeleri olsun. S ve T kümelerinin cebirsel toplamı ve cebirsel farkı sırasıyla aşağıdaki gibi tanımlanır: (Jahn, 2011; Rockafellar, 1970)

$$S + T := \{x + y : x \in S \, ve \, y \in T\}$$

$$S - T := \{x - y : x \in S \, ve \, y \in T\}.$$

Keyfi bir $\lambda \in \mathbb{R}$ için $\lambda S := \{\lambda x : x \in S\}$'dir.

Tanım 1.3: X bir reel normlu uzay olsun. X üzerindeki tüm reel değerli lineer fonksiyonellerin kümesi X^a ile gösterilsin. $\varphi, \psi \in X^a$ ve $\lambda \in \mathbb{R}$ için toplama ve skalerle çarpma işlemleri aşağıdaki gibi tanımlanır (Schaefer ve Wolff, 1999):

$$(\varphi + \psi)(x) = \varphi(x) + \psi(x), \quad \forall x \in X$$

$$(\lambda\varphi)(x) = \lambda\varphi(x), \quad \forall x \in X$$

Bu işlemlerle X^a bir reel lineer uzaydır ve X'in cebirsel duali olarak adlandırılır. $(X^a)^a$, X'in ikinci cebirsel dualidir. Sürekli lineer fonksiyonellerden oluşan $X^* \subseteq X^a$ uzayı ise X'in topolojik dualidir. Bu bölümde dual koni ve subdiferansiyel tanımlarında X^* gösterimi kullanılacaktır.

Tanım 1.4: X bir reel normlu uzay ve $\emptyset \neq S \subseteq X$ olsun (Jahn, 2011; Rockafellar, 1970).

a) $\bar{x} \in S$ verilsin. Her $x \in S$ ve her $\lambda \in [0,1]$ için $\lambda x + (1 - \lambda)\bar{x} \in S$ ise S kümesine $\bar{x}$ noktasında yıldız şekilli denir.
b) Her $x, y \in S$ ve her $\lambda \in [0,1]$ için $\lambda x + (1 - \lambda)y \in S$ ise S kümesi konveks olarak adlandırılır
c) S kümesi boştan farklı ve her $\alpha \in [-1,1]$ için $\alpha S \subset S$ ise S kümesine dengeli küme denir.
d) S kümesi konveks ve dengeli ise mutlak konveks olarak adlandırılır.
e) Bir $\bar{x} \in S$ noktası için her $v \in X$ doğrultusunda, tüm $t \in [0,\varepsilon]$ değerleri için $\bar{x} + tv \in S$ olacak şekilde bir $\varepsilon > 0$ varsa $\bar{x}$, S'nin cebirsel iç noktasıdır.

S'nin tüm cebirsel iç noktalarının kümesine cebirsel iç veya kor denir ve cor(S) ile gösterilir.

Tanım 1.5: X bir reel normlu uzay ve $\emptyset \neq C \subseteq X$ olsun (Jahn, 2011).

Gösterim notu: Sıfır vektörü {0_X} ile gösterilir; pointed koni koşulu $C \cap (-C) = 0_X$ biçimindedir.

a) Her $x \in C$ ve her $\lambda \geq 0$ için $\lambda x \in C$ ise C kümesine bir koni denir.
b) Eğer $C \cap (-C) = 0_X$ ise C konisine pointed koni denir.
c) Eğer $C - C = X$ ise C konisine yeniden üretilen koni denir.
d) $C \neq \{0_X\}$ konveks bir koni ve $\emptyset \neq B \subseteq C \setminus \{0_X\}$ konveks olsun. Her $x \in C \setminus \{0_X\}$ elemanı, bir tek $\lambda > 0$ ve bir tek $b \in B$ ile $x = \lambda b$ biçiminde yazılabiliyorsa B kümesine C konisinin bir tabanı denir.

Tanım 1.6: X bir reel lineer uzay olsun (Jahn, 2011; Schaefer ve Wolff, 1999).

a) $X \times X$ çarpım uzayının her bir R alt kümesi X üzerinde bir bağıntı olarak adlandırılır.
b) X üzerinde tanımlı bir $\leq$ bağıntısı, her x, y, z ∈ X için aşağıdaki koşulları sağlıyorsa bir kısmi sıralama bağıntısıdır:

i. $x \leq x$;
ii. $x \leq y$ ve $y \leq z \Rightarrow x \leq z$;
iii. $x \leq y$ ve $y \leq x \Rightarrow x = y$.
iv. Ayrıca her x, y, w, z ∈ X ve $\alpha \geq 0$ için $x \leq y$, $w \leq z \Rightarrow x + w \leq y + z$ ve $x \leq y \Rightarrow \alpha x \leq \alpha y$ koşulları sağlanıyorsa sıralama lineer yapı ile uyumludur.

c) Bu durumda X, kısmi sıralı bir reel lineer uzay olarak adlandırılır. Antisimetri koşulu çıkarılırsa elde edilen bağıntı bir ön sıralama bağıntısıdır.

Tanım 1.7: X bir reel normlu uzay ve $C \subseteq X$ konveks bir koni olsun. $x \leq_C y \Leftrightarrow y - x \in C$ bağıntısı toplama ve negatif olmayan skalerle çarpma ile uyumlu bir ön sıralamadır. Bu bağıntı $C \cap (-C) = \{0_X\}$ olduğunda bir kısmi sıralamadır; bu durumda C sıralama konisi olarak adlandırılır (Jahn, 2011).

Açıklama: Konvekslik ve koniye göre sıralama birbirinden farklı özelliklerdir. Örneğin reel düzlemde $C = \mathbb{R}^2_+$ seçildiğinde (1, 2) ve (2, 1) noktaları bu sıralamaya göre karşılaştırılamaz. Dolayısıyla kısmi sıralama, bütün vektörlerin karşılaştırılmasını gerektirmez.

Tanım 1.8: X bir reel normlu uzay, X* topolojik dual uzayı ve $C \subseteq X$ konveks bir koni olsun (Jahn, 2011).

a) $C_{X^*} := \{x^* \in X : x^*(x) \geq 0, \forall x \in C_X\}$

kümesine C'nin dual konisi denir. $x^* \leq_{C^*} y^* \Leftrightarrow y^* - x^* \in C^*$ bağıntısı dual uzayda bir ön sıralama tanımlar. Bu bağıntının kısmi sıralama olması için C*'ın pointed olması gerekir. Ayrıca

a) $C^{\#}_{X^*} := \{x^* \in X : x^* \in X(x) > 0, \forall x \in C_X \setminus 0_X\}$

kümesi, C'nin sıfırdan farklı elemanları üzerinde kesin pozitif olan sürekli lineer fonksiyonellerden oluşur ve dual koninin quasi-içi olarak adlandırılır. Genel olarak $C^{\#}_{X^*}$ ile C_{X^*}'ın topolojik içi aynı olmak zorunda değildir.

Normlar ve Sıralama Konileri

Örnek: $X = \mathbb{R}^2$ ve $C = \mathbb{R}^2_+$ için dual koni yine $\mathbb{R}^2_+$ olur. Gerçekten, (a, b) doğrusal fonksiyonelinin C üzerindeki bütün noktalarda negatif olmayan değer alması ancak $a \geq 0$ ve $b \geq 0$ olduğunda mümkündür. Bu örnek, dual koninin sıralama bilgisini doğrusal fonksiyoneller aracılığıyla nasıl taşıdığını gösterir.

Tanım 1.9: X ve Y reel lineer uzaylar, $C_Y \subseteq Y$ konveks ve pointed bir koni olsun. Her x, y ∈ X ve her λ ∈ ℝ için aşağıdaki koşulları sağlayan p: X → C_Y dönüşümüne vektörel norm denir (Jahn, 2011; Schaefer ve Wolff, 1999):

a) $p(x) \geq_{C_Y} 0_Y$;
b) $p(x) = 0_Y \Leftrightarrow x = 0_X$;
c) $p(\lambda x) = |\lambda| p(x)$;
d) $p(x + y) \leq_{C_Y} p(x) + p(y)$.

Özel olarak $Y = \mathbb{R}$ ve $C_Y = \mathbb{R}_+$ ise p bir normdur ve $\|\cdot\|$ ile gösterilir; $(X, \|\cdot\|)$ bir reel normlu uzaydır. Kesin pozitiflik koşulu yerine yalnızca $p(0_X) = 0_Y$ koşulu aranırsa p, vektörel yarınorm olarak adlandırılır. Reel değerli durumda bu kavram alışılmış yarınorm tanımına karşılık gelir.

Tanım 1.10: X bir reel topolojik vektör uzayı ve $C \subseteq X$ bir sıralama konisi olsun. C'ye göre bir alt sınıra sahip her azalan ağ, yani

$$i \leq j \Rightarrow x_j \leq_C x_i$$

koşulunu sağlayan her ağ, X'te bir infimuma sahip oluyor ve bu infimuma yakınsıyorsa C konisine Daniell konisi denir (Jahn, 2011).

Dönüşümler, Koniler ve Küme Değerli Analiz

Tanım 1.11: X ve Y reel lineer uzaylar ve T: X → Y bir dönüşüm olsun. Her x, y ∈ X ve her λ, μ ∈ ℝ için (Schaefer ve Wolff, 1999)

$$T(\lambda x + \mu y) = \lambda T(x) + \mu T(y)$$

ise T dönüşümüne bir lineer dönüşüm denir.

Tanım 1.12: X ve Y reel lineer uzaylar, $C_Y \subseteq Y$ konveks bir koni, $\emptyset \neq S \subseteq X$ konveks bir küme ve f: S → Y bir dönüşüm olsun. Her x, y ∈ S ve her λ ∈ [0,1] için (Jahn, 2011)

$$\lambda f(x) + (1 - \lambda) f(y) - f(\lambda x + (1 - \lambda) y) \in C_Y$$

koşulu sağlanıyorsa f, C_Y-konveks olarak adlandırılır. C_Y sıralama konisi olduğunda bu koşul aşağıdaki gibi yazılabilir:

$$f(\lambda x + (1 - \lambda) y) \leq_{C_Y} \lambda f(x) + (1 - \lambda) f(y)$$

Bu iki ifade eşdeğerdir.

Tanım 1.13: X ve Y reel normlu uzaylar, $C_Y \subseteq Y$ konveks ve pointed bir koni, $\emptyset \neq S \subseteq X$ ve $f: S \to Y$ bir dönüşüm olsun (Jahn, 2011; Rockafellar, 1970).

Gösterim açıklaması: Tek değerli f için f(x)+C ifadesi $\{f(x)\} + C$ anlamındadır. Dolayısıyla $(x, y) \in epi(f)$ olması, $y - f(x) \in C$ koşuluna eşdeğerdir.

$$epi(f) \coloneqq \{(x, y): x \in S, y \in f(x) + C_Y\}$$

ile tanımlanan kümeye f dönüşümünün üst grafiği denir.

$$epi(f) \coloneqq (x, y): x \in S, f(x) \leq_{C_Y} y$$

olarak da yazılabilir.

Tanım 1.14: S, bir ≤ kısmi sıralama bağıntısına sahip boş olmayan bir küme olsun (Jahn, 2011; Schaefer ve Wolff, 1999).

Aşağıdaki maksimal ve minimal eleman koşulları, S kümesindeki her x elemanı için değerlendirilir. Kısmi sıralamanın antisimetri özelliği nedeniyle, maksimal bir elemandan kesin büyük; minimal bir elemandan ise kesin küçük başka bir eleman bulunamaz.

a) Her $x, y \in S$ için ya $x \leq y$ ya da $y \leq x$ ise S kümesine tam sıralı denir.
b) T kümesi S kümesinin boş olmayan bir alt kümesi olsun. Her x ∈ T için

$$x \leq \bar{x}$$

ise $\bar{x} \in S$ elemanı T'nin bir üst sınırı olarak adlandırılır.

c) Her x ∈ T için

$$\bar{x} \leq x$$

ise x̄ ∈ S elemanı T'nin bir alt sınırı olarak adlandırılır.

d) $x \in S, \bar{x} \leq x \Rightarrow x \leq \bar{x}$

ise x̄ ∈ S elemanı S'nin bir maksimal elemanı olarak adlandırılır.

e) $x \in S, x \leq \bar{x} \Rightarrow \bar{x} \leq x$

ise $\bar{x} \in S$ elemanı S'nin bir minimal elemanı olarak adlandırılır.

Tanım 1.15: X bir reel normlu uzay, ∅ ≠ S ⊆ X, x̄ ∈ S ve f: S → ℝ bir fonksiyon olsun (Rockafellar, 1970).

$$f(\bar{x}) \leq lim\, inf_\{x \to \bar{x}, x \in S\} f(x)$$

koşulu sağlanıyorsa f fonksiyoneline $\bar{x} \in S$ noktasında alttan yarı sürekli denir.

Tanım 1.16: Z bir reel normlu uzay, $\emptyset \neq U \subseteq Z$ ve $\bar{z} \in cl(U)$ olsun. U içinde bir (u_n) dizisi ile sıfıra azalarak yakınsayan pozitif sayıların bir (t_n) dizisi için (Aubin ve Frankowska, 2009)

$$u_n \to \bar{z}, \quad t_n \downarrow 0, \quad (u_n - \bar{z})/t_n \to z$$

koşulları sağlanıyorsa $z \in Z$ vektörüne U'nun $\bar{z}$ noktasında bir tanjant vektörü denir. Bu vektörlerin kümesi U'nun $\bar{z}$ noktasındaki contingent konisi veya Bouligand tanjant konisi olarak adlandırılır ve $T(U, \bar{z})$ ile gösterilir.

Tanım 1.17: Z bir reel normlu uzay, $\emptyset \neq U \subseteq Z$ ve $\bar{z} \in cl(U)$ olsun. U'nun $\bar{z}$ noktasındaki kapalı radyal konisi, aşağıdaki biçimde tanımlanır (Aubin ve Frankowska, 2009; Jahn, 2011):

$$R(U, \bar{z}) := cl(cone(U - \bar{z})).$$

$$cone(U - \bar{z}) := \{\lambda(u - \bar{z}) : \lambda \geq 0, u \in U\}.$$

Burada cone gösterimi konik zarfı değil, yukarıdaki radyal doğrultular kümesini ifade eder. Tanım, pozitif (λ_n) ve U içinde (u_n) dizileri kullanılarak eşdeğer olarak aşağıdaki gibi yazılabilir:

$$z \in R(U, \bar{z}) \Leftrightarrow \exists\, \lambda_n > 0, \exists\, u_n \in U: \lambda_n(u_n - \bar{z}) \to z.$$

Eşdeğer olarak $z \in R(U, \bar{z})$ olması, pozitif (s_n) ve Z içinde (v_n) dizileri için aşağıdaki koşulların sağlanması demektir:

$$v_n \to z, \quad \bar{z} + s_n v_n \in U, \quad \forall\, n \in \mathbb{N}.$$

Contingent konide taban noktaya yaklaşma koşulu bulunurken radyal konide yukarıdaki u_n dizisinin $\bar{z}$ noktasına yakınsaması gerekmez. Bu nedenle her zaman

$$T(U, \bar{z}) \subseteq R(U, \bar{z})$$

sağlanır.

Örnek 1 (contingent ve kapalı radyal konilerin farkı): $Z = \mathbb{R}^2$, $U = \{(0,0), (1,0)\}$ ve $\bar{z} = (0,0)$ olsun. $\bar{z}$ noktası U içinde yalıtılmış olduğundan contingent koni yalnızca sıfır vektöründen oluşur: $T(U, \bar{z}) = \{(0,0)\}$. Buna karşılık kapalı radyal koni $R(U, \bar{z}) = \{(t, 0): t \geq 0\}$ kümesidir. Böylece $T(U, \bar{z}) \subsetneq R(U, \bar{z})$ elde edilir. Bu örnekte radyal koni, taban noktaya yaklaşan noktalarla sınırlı kalmadığı için daha fazla yön içerir.

Tanım 1.18: X ve Y reel normlu uzaylar ve $F: X \rightrightarrows Y$ küme değerli bir dönüşüm olsun. F'nin grafiği ve tanım kümesi sırasıyla aşağıdaki gibi tanımlanır (Aubin ve Frankowska, 2009; Jahn ve Rauh, 1997):

a) $graph(F) \coloneqq (x, y) \in X \times Y : y \in F(x)$;

ve

b) $dom(F) \coloneqq x \in X : F(x) \neq \emptyset$.

Y'nin konveks ve pointed bir C ⊆ Y konisi ile kısmi sıralı olduğunu varsayalım. F'nin C'ye göre üst grafiği

c) aşağıdaki kümedir:

$$epi(F) \coloneqq (x, y) \in X \times Y : y \in F(x) + C.$$

$(\bar{x}, \bar{y}) \in graph(F)$ olsun ve $K \coloneqq T(epi(F), (\bar{x}, \bar{y}))$ yazılsın. $D \coloneqq \{u \in X : \exists\, v \in Y, (u, v) \in K\}$, K'nin X üzerindeki izdüşümü olsun.

d) Üst grafiği K'ye eşit olan tek değerli bir $DF(\bar{x}, \bar{y}): D \to Y$ dönüşümü varsa, yani

$$epi(DF(\bar{x}, \bar{y})) = T(epi(F), (\bar{x}, \bar{y})),$$

bu dönüşüme F'nin ($\bar{x}$,$\bar{y}$) noktasındaki contingent üst türevi denir. Bu türevin varlığı her küme değerli dönüşüm için garanti edilmez; tanım alanı da genel olarak X'in tamamı değildir (Jahn ve Rauh, 1997).

Açıklama: Üst grafik, küme değerli dönüşümün değerlerini sıralama konisi yönünde genişletir. Bu nedenle grafiğin geometrisi ile üst grafiğin geometrisi farklı olabilir. Contingent üst türev tanımında esas alınan yapı doğrudan graph(F) değil, epi(F) kümesinin contingent konisidir; ayrıca bu koninin tek değerli bir dönüşümün üst grafiği olarak temsil edilebilmesi gerekir.

Tanım 1.19: Y bir reel normlu uzay, C ⊆ Y konveks ve pointed bir koni ve ∅ ≠ A ⊆ Y olsun. Her y ∈ A için a $\leq_C$ y, yani y − a ∈ C koşulu sağlanıyorsa a ∈ Y, A'nın bir alt sınırıdır. Alt sınırın A'ya ait olması gerekmez. A'nın alt sınırları arasında en büyük eleman varsa buna A'nın infimumu denir ve inf A ile gösterilir. İnfimum her küme için var olmak zorunda değildir (Jahn, 2011).

Tanım 1.20: Y bir reel normlu uzay, C ⊆ Y kapalı, konveks ve pointed bir koni, ∅ ≠ A ⊆ Y ve y ∈ A olsun (Jahn, 2011).

a) $A \cap (\{y\} - C) = \{y\}$ ise y elemanı A kümesinin minimal elemanı olarak adlandırılır.

b) int(C) ≠ ∅ olsun. A ∩ ({y} − int(C)) = ∅ koşulu sağlanıyorsa y, A'nın zayıf minimal elemanı olarak adlandırılır.

c) y ∈ A minimal olsun. R(A + C,y) ∩ (−C) = $\{0_Y\}$ koşulu sağlanıyorsa y, Benson anlamında has minimal eleman olarak adlandırılır. Burada R(A + C,y) = cl(cone(A + C − {y}))'dir. A'nın C'ye göre minimal, zayıf minimal ve has minimal elemanlarının kümeleri sırasıyla Min(A,C), WMin(A,C) ve PMin(A,C) ile gösterilir.

Örnek 2 (minimal ve zayıf minimal noktalar): Y = $\mathbb{R}^2$, C = $\mathbb{R}^2_+$ ve $A = \{(0,1),(1,0),(1,1)\}$ olsun. $(0,1)$ ve $(1,0)$ minimaldir; $(1,1)$ minimal değildir, çünkü diğer iki nokta tarafından C sıralamasında domine edilir. Buna karşılık $(1,1)$ zayıf minimaldir: A içinde her iki koordinatı da kesin olarak daha küçük olan bir nokta bulunmaz. Bu ayrım, zayıf minimalitenin minimaliteden daha geniş bir kavram olduğunu gösterir.

Tanım 1.21: X bir reel normlu uzay, X* topolojik dual uzayı, F: X → $\mathbb{R}$ bir fonksiyon ve $\bar{x}$ ∈ X olsun. Her x ∈ X için (Rockafellar, 1970)

$$F(x) - F(\bar{x}) \geq \langle x*, x - \bar{x} \rangle$$

eşitsizliğini sağlayan x* ∈ X* fonksiyoneline F'nin $\bar{x}$ noktasındaki (konveks analiz anlamında) subgradienti denir. Bu fonksiyonellerin kümesi F'nin $\bar{x}$ noktasındaki subdiferansiyelidir ve $\partial F(\bar{x})$ ile gösterilir. Burada ⟨x*,x⟩ = x*(x) dual eşleşmesini belirtir. Bu tanım global bir destekleme eşitsizliğine dayanır; genel bir fonksiyonun subdiferansiyeli boş olabilir.

Sonuç

Bu bölümde küme değerli analizin temel kavramları, cebirsel ve sıralamaya ilişkin yapılar çerçevesinde bir araya getirilmiştir. Lineer uzaylar, konveks kümeler ve konilerden hareketle dual yapılar, vektörel normlar ve Daniell konisi ele alınmış; ardından dönüşümlerin grafikleri ve üst grafikleri ile contingent ve kapalı radyal koniler tanımlanmıştır. Bu düzen, küme değerli dönüşümlerin incelenmesinde kullanılan kavramlar arasındaki ilişkileri ortaya koymaktadır.

Koniye bağlı sıralama, vektör değerlerinin karşılaştırılmasına olanak verirken minimal, zayıf minimal ve has minimal eleman tanımları farklı optimalite anlayışlarını ifade etmektedir. Üst grafik ve teğet koni yapıları türev kavramlarının geometrik temellerini; subdiferansiyel ise reel değerli fonksiyonların destekleyici lineer fonksiyoneller aracılığıyla incelenmesini ortaya koymaktadır. Sunulan tanımlar, küme değerli türevler, skalerleştirme ve optimalite koşulları üzerine yapılacak ileri çalışmalar için bir başlangıç çerçevesi sağlamaktadır.

Tanımların ardından verilen örnekler, sıralama konilerinin karşılaştırma üzerindeki etkisini ve contingent koni ile kapalı radyal koninin her zaman çakışmadığını somutlaştırmaktadır.

Anahtar Kelimeler: Küme değerli analiz, konveks koni, kısmi sıralama, contingent koni, radyal koni, minimal eleman, subdiferansiyel.

KAYNAKÇA

Aubin, J.-P., & Frankowska, H. (2009). Set-valued analysis. Birkhäuser. https://doi.org/10.1007/978-0-8176-4848-0

Jahn, J. (2011). Vector optimization: Theory, applications, and extensions (2nd ed.). Springer. https://doi.org/10.1007/978-3-642-17005-8

Jahn, J., & Rauh, R. (1997). Contingent epiderivatives and set-valued optimization. Mathematical Methods of Operations Research, 46(2), 193–211. https://doi.org/10.1007/BF01217690

Rockafellar, R. T. (1970). Convex analysis. Princeton University Press.

Schaefer, H. H., & Wolff, M. P. (1999). Topological vector spaces (2nd ed.). Springer. https://doi.org/10.1007/978-1-4612-1468-7